Title
MicroRNA-23a promotes myelination in the central nervous system.

Journal
Proceedings of the National Academy of Sciences of the United States of America, 110(43)

ISSN
0027-8424

Authors
Lin, Shu-Ting
Huang, Yong
Zhang, Luoying
et al.

Publication Date
2013-10-01

DOI
10.1073/pnas.1317182110

Peer reviewed

MicroRNA-23a promotes myelination in the central nervous system

Shu-Ting Lin[a], Yong Huang[a,b], Luoying Zhang[a], Mary Y. Heng[a], Louis J. Ptáček[a,b,1], and Ying-Hui Fu[a,1]

[a]Department of Neurology and [b]Howard Hughes Medical Institute, University of California, San Francisco, CA 94158

Contributed by Louis J. Ptáček, September 17, 2013 (sent for review August 6, 2013)

Demyelinating disorders including leukodystrophies are devastating conditions that are still in need of better understanding, and both oligodendrocyte differentiation and myelin synthesis pathways are potential avenues for developing treatment. Overexpression of lamin B1 leads to leukodystrophy characterized by demyelination of the central nervous system, and microRNA-23 (*miR-23*) was found to suppress lamin B1 and enhance oligodendrocyte differentiation in vitro. Here, we demonstrated that *miR-23a*–overexpressing mice have increased myelin thickness, providing in vivo evidence that *miR-23a* enhances both oligodendrocyte differentiation and myelin synthesis. Using this mouse model, we explored possible *miR-23a* targets and revealed that the phosphatase and tensin homologue/phosphatidylinositol trisphosphate kinase/Akt/mammalian target of rapamycin pathway is modulated by *miR-23a*. Additionally, a long noncoding RNA, *2700046G09Rik*, was identified as a *miR-23a* target and modulates phosphatase and tensin homologue itself in a *miR-23a*–dependent manner. The data presented here imply a unique role for *miR-23a* in the coordination of proteins and noncoding RNAs in generating and maintaining healthy myelin.

MicroRNAs (miRNAs) play an important role in regulating a large number of developmental processes and diseases (1–3) through fine tuning biological networks (4, 5). Expression levels of miRNAs in oligodendroglia vary according to their differentiation stages, indicating a possible role for miRNAs in regulating developmental processes among migratory, proliferating, and myelinating oligodendrocytes (OLs) (6–9). Disruption of miRNA biogenesis by *Dicer* ablation in oligodendroglia at postdevelopmental stages results in a neurodegenerative phenotype including demyelination, inflammation, and axon loss (10), suggesting that miRNAs are also important for myelin maintenance at later developmental stages. *miR-23* is among the most abundant miRNAs in OLs (6, 7). Previously, we reported that in the presence of excess *miR-23* in vitro, a greater proportion of cells express mature markers of OLs that are paralleled by multipolar morphological appearance with increased levels of mature myelin proteins, indicating that *miR-23* can enhance oligodendrogenesis (11). In contrast, excessive lamin B1, a nuclear envelope protein and target of *miR-23*, leads to lower numbers of cells expressing mature markers with reduced levels of mature myelin proteins both in vitro and in vivo, suggesting defective differentiation of OLs. Importantly, the adverse effects of lamin B1 on OL cells can be abrogated by overexpressing *miR-23*, which functions as a negative regulator of lamin B1.

Here, we use mice in which *miR-23a* (one of the two *miR-23* isoforms: *miR-23a* and *b*) overexpression is driven by an OL-specific promoter [*2′,3′-cyclic nucleotide 3′-phophodiesterase* (*Cnp*)] to investigate the effects of *miR-23a* on OL differentiation and myelin synthesis in vivo. We demonstrated that in addition to the previously identified target, lamin B1, *miR-23a* also directly modulates the expression of two targets—phosphatase and tensin homolog on chromosome 10 (*PTEN*) and a long noncoding RNA (lncRNA), *2700046G09Rik* (RIKEN cDNA 2700046G09 gene). Through modulating expression of these molecules in myelinating glia cells, *miR-23a* fine tunes activities of the serine-threonine protein kinase Akt/mTOR (mechanistic target of rapamycin) and mitogen-associated protein kinase (MAPK) pathways that promote expression of myelin genes. Our results indicate that myelination requires tightly regulated multilayer signaling pathways partly converging downstream of PIP3 (phosphatidylinositol-3,4,5-trisphosphate) with coordinated nuclear changes such as transcription to trigger myelin gene expression, which then leads to proper membrane wrapping of axons by OLs.

Results

Generation of Transgenic Mice Overexpressing *miR-23a* in Oligodendrocytes. We have previously shown that *miR-23* overexpression enhances OL maturation in an established culture system (11). In addition, *miR-23a* and *miR-23b* are both up-regulated in OL under differentiation conditions compared with progenitor status under proliferation conditions (Fig. S1*A*). Knockdown of both *miR-23a* and *miR-23b* leads to significant reductions, whereas knockdown of either *miR-23a* or *miR-23b* individually does not cause obvious changes in expression levels of myelin genes (Fig. S1*B*), suggesting that *miR-23a* and *miR-23b* can compensate for each other in regulating OL maturation. Immunoreactivity of myelin basic protein (MBP) also demonstrated that *miR-23a* and *miR-23b* together had stronger effects on MBP expression than either one alone (Fig. S1 *C* and *D*). Given that ectopic expression of *miR-23* can promote transcription of myelin genes in cultured glia and purified OLs, we investigated the impact of overexpressing *miR-23a* on myelin formation in vivo. Northern blot analyses demonstrated that *miR-23a* displays reduced expression in *Dicer1*-ablated neurons, oligodendrocytes, and astrocytes (Fig. S2*A*), indicating ubiquitous expression of *miR-23a* in the CNS. Murine *Cnp* promoter was used to generate *miR-23a* transgenic mice (Fig. S2 *B* and *C*), as *Cnp* is highly expressed in developing OLs (12). Seven *Cnp–miR-23a* founder lines demonstrated *miR-23a* overexpression (Fig. S2*D*) and three of these lines with different expression levels were selected for further characterization. Quantitative RT-PCR

Significance

Understanding molecular mechanisms that underlie the processes for myelin synthesis and maintenance has been an intensely investigated topic. Concurrently, recent advances in noncoding RNAs (ncRNAs) have uncovered unique insights into many biological processes, and ncRNAs have become recognized as major players for epigenetic regulation. We generated a murine model overexpressing microRNA-23a (*miR-23a*) to investigate its role in myelin regulation. In addition, we used this mouse model to identify two targets of *miR-23a*: one is a protein-coding gene phosphatase and tensin homologue and the other is a long ncRNA (lncRNA) *2700046G09Rik*. Our study demonstrated a complex network comprising a protein-encoding gene, a miRNA, and a lncRNA that is central to the fine tuning and maintenance of healthy myelin.

Author contributions: S.-T.L., L.Z., M.Y.H., L.J.P., and Y.-H.F. designed research; S.-T.L. and L.Z. performed research; S.-T.L. and Y.H. analyzed data; and S.-T.L., Y.H., L.J.P., and Y.-H.F. wrote the paper.

The authors declare no conflict of interest.

[1]To whom correspondence may be addressed. E-mail: ljp@ucsf.edu or ying-hui.fu@ucsf.edu.

This article contains supporting information online at www.pnas.org/lookup/suppl/doi:10.1073/pnas.1317182110/-/DCSupplemental.

(qRT-PCR) of oligodendrocyte progenitor cells (OPCs) purified from two lines display moderate-to-high levels of *miR-23a* in proliferative medium and a further significant increase in differentiation medium (Fig. S2*E*). *Cnp–miR-23a* mice carrying one transgene allele were not overtly distinguishable from control littermates but mice carrying two transgene alleles developed a notable unilateral hindlimb paralysis as early as postnatal day 5 (P5) (Fig. 1*A*). In addition, these *Cnp–miR-23a* mice exhibited abnormal axial muscle tone (kyphosis), puffy eyes, and hindlimb ataxia from P42 (Fig. 1*A*).

Because there is no standard behavioral analysis specifically designed for myelin assessment (13), we used several tests to examine the *Cnp–miR-23a* mice for neurological dysfunction. We examined general locomotor activity of mice at 20 wk of age. *Cnp–miR-23a* transgenic mice showed motor impairment by requiring more time to traverse the balance beam (5 mm and 11 mm) (Fig. 1*B*) and a higher rate of hindlimb slips and dragging (Fig. S3 *A* and *B*). The hanging wire test was next used to examine whether the motor impairments were related to loss of muscle power, and significant differences were observed (Fig. 1*C*). Additionally, *Cnp–miR-23a* mice required more time to traverse the diagonal bar (Fig. 1*D*) and displayed a lower success rate (Fig. 1*E*) as well as reduced duration on the coat hanger (Fig. S3*C*), supporting that *Cnp–miR-23a* mice exhibited impaired motor function, which is likely a neurological consequence of *miR-23a* overexpression in OLs.

***miR-23a* Regulates Oligodendrocyte Differentiation.** To determine whether overexpressing *miR-23a* affects OL differentiation in vivo, oligodendroglia from transgenic mice under proliferation or differentiation conditions were used to analyze the expression levels of myelin genes. Interestingly, many of the myelin genes [particularly late phase genes such as myelin-associated glycoprotein (*Mag*), transferrin (*Trf*), and myelin oligodendrocyte glycoprotein (*Mog*)] are simultaneously up-regulated in *miR-23a* OLs compared with wild-type (WT) control cultures (Fig. 2*A*). Early OL gene such as proteolipid protein (*Plp*) and *Mbp* were also induced to a mild extent by *miR-23a* overexpression under proliferation conditions (Fig. S3*D*). *miR-23a* overexpression not only increased the number of OLs expressing MBP and MAG (Fig. 2*B* and Fig. S3*E*), but also increased the overall expression of PLP and MBP compared with control oligodendroglia (Fig. 2*C*), supporting *miR-23a* as a key regulator of OL differentiation.

Overexpression of *miR-23a* Leads to Enhanced Myelination in the Central Nervous System. Increased myelination in *Cnp–miR-23a* mice compared with WT control was observed in the corpus callosum stained with myelin-specific dye and CNP/MBP

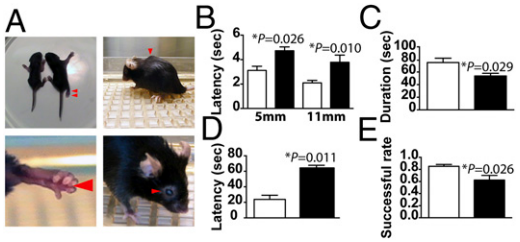

Fig. 1. *Cnp–miR-23a* mice exhibited impaired motor function. (*A*) Morphological abnormalities displayed in *Cnp–miR-23a* mice: hindlimb paralysis (*Upper Left*), loss of foot extensor tone (*Lower Left*), kyphosis (*Upper Right*) and puffy eyes (*Lower Right*). Mice at the age of P150 were analyzed with balanced beam test (*B*), horizontal wire hanging test (*C*), and coat hanger test (*D* and *E*). Measurement of time for *Cnp–miR-23a* mice to traverse balance beams (*B*) and to hang in horizontal wire (*C*) and measurement of latency to reach the diagonal bar (*D*) and successful rate to reach diagonal bar (*E*) are shown. Data are presented as means ± SEM, $n = 7$ per genotype, $^*P < 0.05$, unpaired Student *t* test. Filled bars represent *Cnp–miR-23a* and open bars denote WT mice.

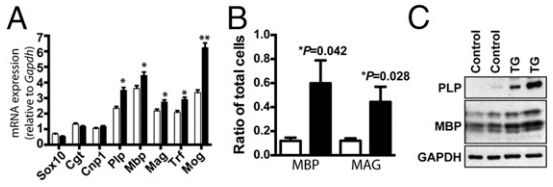

Fig. 2. Overexpressing *miR-23a* promotes OPC differentiation. (*A*) Expression of OL markers in cells purified from P7 *Cnp–miR-23a* mice was assessed using qRT-PCR. Data are presented as means ± SEM, $^*P < 0.05$, $^{**}P < 0.01$, unpaired Student *t* test. $n = 4$ per genotype. Filled bars represent *Cnp–miR-23a* OLs and open bars denote WT OLs. (*B*) Quantification of MBP- or MAG-positive cells in OPCs purified from P7 WT and *Cnp–miR-23a* mice cultured for 4 d in vitro (DIV) in differentiation medium. The total numbers of cells were determined by DAPI staining. Data are presented as ratio ± SEM from three independent experiments. $^*P < 0.05$. (*C*) Representative Western analyses showed increased expression of PLP and MBP in *Cnp–miR-23a* OLs relative to control. Protein lysates were purified from OPCs cultured at 4 DIV in differentiation media. GAPDH was used as a loading control.

antibodies (Fig. 3*A*). The size of the corpus callosum was increased in *Cnp–miR-23a* mice at P90. Expression of myelin proteins, such as CNP, MBP, and MAG was elevated (Fig. 3*B*). Electron microscopy (EM) analysis revealed an increased number of axons exhibiting focal myelin pathology such as aberrant myelin outfoldings caused by hypermyelination at P180 (Fig. 3 *C* and *D*, yellow and green arrowheads) or "invaginating" recurrent loops (Fig. 3*D*, red arrowhead), which showed similar features with the myelin sheath from which they had originated. We quantified the myelin abnormalities by comparing electron microscopy of rostral corpus callosum from *Cnp–miR23a* and controls at 6 mo of age. G ratios for the transgenic $(TG)^+/WT^-$ or TG^+/TG^+ *Cnp–miR-23a* mice are 0.6144 (±0.0043) and 0.6366 (±0.0045), respectively, which are significantly different from controls (0.7088 ± 0.0038) (Fig. 3*E*, *Upper Right*, $P < 0.01$). Increased myelin thickness was evident for axons of small calibers (Fig. 3*E*, *Upper Left*), but not all fibers were visibly hypermyelinated. The overall size distribution of callosal axons was similar in transgenic and control mice (Fig. 3*E*, *Lower*). EM demonstrated increased layers of myelin sheath wrapping in either small or large caliber axons with increased membrane wraps (Fig. 3*F*). Together, these data implicate *miR-23a* in the regulation of myelin thickness and proper myelin folding in the central nervous system (CNS).

Unbiased Search for *miR-23a* Targeted Molecules and Mechanisms. To further investigate the mechanisms of *miR-23a* in OL development and myelination, we set out to identify other relevant targets that are regulated by *miR-23a*. A total of 1,179 genes were identified to demonstrate differential expression between *Cnp–miR-23a* and WT mice [absolute fold change (FC) >1.5, multitest adjusted *P* value ≤0.05 correspondent to unadjusted *P* value ≤0.013 by cufflink] (Fig. 4*A* and Datasets S1 and S2). This included many known myelin-formation–associated genes, which were highly expressed in *Cnp–miR-23a* (Fig. 4*B*). Additionally, we found that genes specific to early stages of oligodendroglia development, such as *Pdgfra* and *Lmnb1*, displayed reduced levels in OLs purified from *Cnp–miR-23a*.

Next, we compared the differentially expressed genes with the reference lists of genes that are enriched in astrocytes, neurons, and OLs (14). The OL-enriched genes are mostly up-regulated in *Cnp–miR-23a*, whereas the neuron-enriched genes tend to be down-regulated (Fig. S4 *C* and *D*). Upon further dissection of *miR-23a* on promoting OL differentiation, we found that genes enriched in more mature OLs, including OLs and the most mature MOG^+ OLs (14), are mostly up-regulated (Fig. 4*C* and Fig. S4*E*). Collectively, the results of RNA sequencing (RNA-Seq) suggest a role for *miR-23a* in promoting the progression of less-differentiated OPCs into myelinating and mature OLs, likely by promoting the expression of mature OL-enriched genes. This

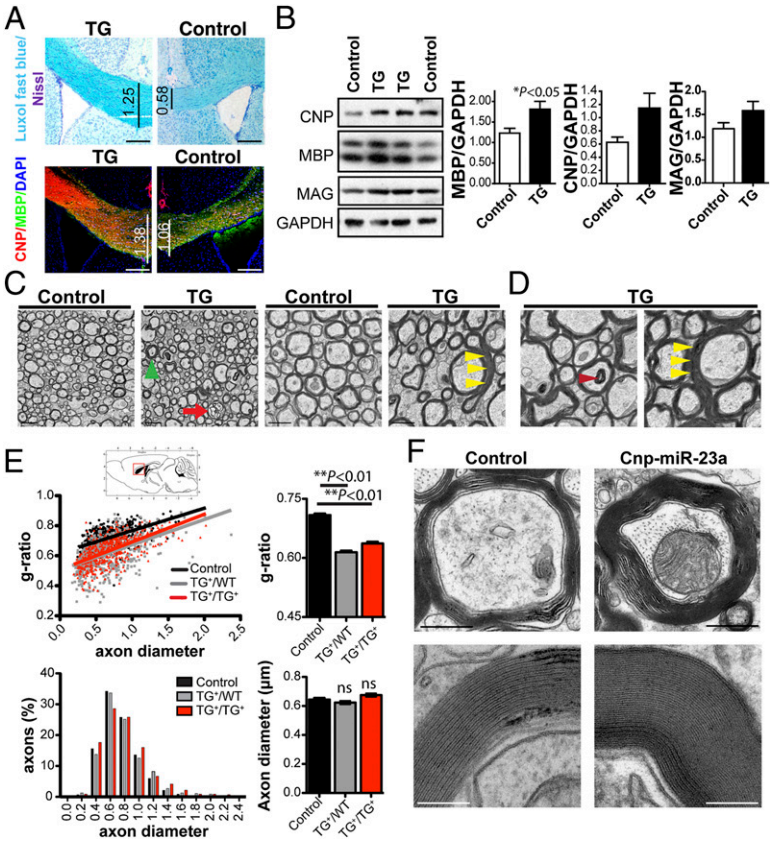

Fig. 3. Enhanced myelination in *Cnp–miR-23a* mice. (*A*) Corpus callosum in WT and *Cnp–miR-23a* mice at P90 showing enhanced myelination by Luxol Fast blue and CNP/MBP immunoreactivities. (*B*) Quantification of MBP, CNP, and MAG in corpus callosum by Western blot analysis ($n = 3$, $^*P < 0.05$, unpaired Student *t* test). (*C* and *D*) Myelin abnormalities in corpus callosum of *Cnp–miR-23a* mice at P180, including hypermyelination (green arrowheads), myelin debris (red arrows), aberrant outfoldings (yellow arrowheads), and invaginating recurrent loops in axons (red arrowhead). [Scale bar for *C*, 1 μm (*Left*) or 2 μm (*Right*)]. (*E*) Quantitation of myelin thickness by modified G-ratio analysis and axon size distribution for the corpus callosum (age, P180; $n = 2$ per genotype; control, WT littermates; TG^+/WT, one allele of transgene; TG^+/TG^+, two alleles of transgene). (*Upper Left*) Scatter plots comparing G ratios from TG^+/WT (gray), TG^+/TG^+ (red), and age-matched controls (black) in relation to myelin sheath inner diameter. (*Upper Right*) Myelin thickness is significantly increased in *Cnp–miR-23a* mice. (*Lower*) Axonal calibers are comparable between *Cnp–miR-23a* mice and controls. ($^{**}P < 0.01$, one-way ANOVA). (*F*) Hypermyelination in *Cnp–miR-23a* mice (*Right*) is caused by additional membrane wraps, as visualized by ultrastructure and periodicity of myelin sheaths. [Scale bar, 500 nm (*Upper*) and 100 nm (*Lower*)].

regulation may be accompanied by repression of neuron-enriched and (to a lesser extent) astrocyte-enriched genes.

***miR-23a* Target Molecules: *PTEN* and *2700046G09Rik*.** *In silico* prediction (miRANDA and TargetScan) followed by luciferase reporter assay was carried out to identify potential direct targets of *miR-23a* for regulating CNS myelination. We reasoned that true *miR-23a*–targeted genes would display positive correlation between RNA-Seq and luciferase reporter analysis. Among 35 candidates examined in this study, *PTEN* and *2700046G09Rik* (Fig. S5*A*) displayed positive correlation. In addition, their genomic locations are rather close, which raised a possibility for the lncRNA (*2700046G09Rik*) to exert *cis*-regulatory effect on the neighboring *PTEN* gene (15). Therefore, we investigated them further. The repression of *PTEN* and enhancement of *2700046G09Rik* by *miR-23a* were validated by mutagenizing their respective *miR-23a* binding elements (Fig. S5 *B–D*) *miR-23* exhibits a gradually increased expression pattern during postnatal development (11), and the true direct target genes of *miR-23a* should display expression patterns correlating with *miR-23a* expression. Indeed, the protein levels of PTEN display a gradual decrease from postnatal day 1 to 10 months of age (Fig. 5*A*), whereas the levels of *2700046G09Rik* display a gradual increase beginning at postnatal day 60 (Fig. 5*B*). We next validated the interaction of *miR-23a* and *PTEN* or *2700046G09Rik* by UV–cross-link RNA immunoprecipitation (RIP) (16). FLAG-AGO2 immunoprecipitation was conducted in

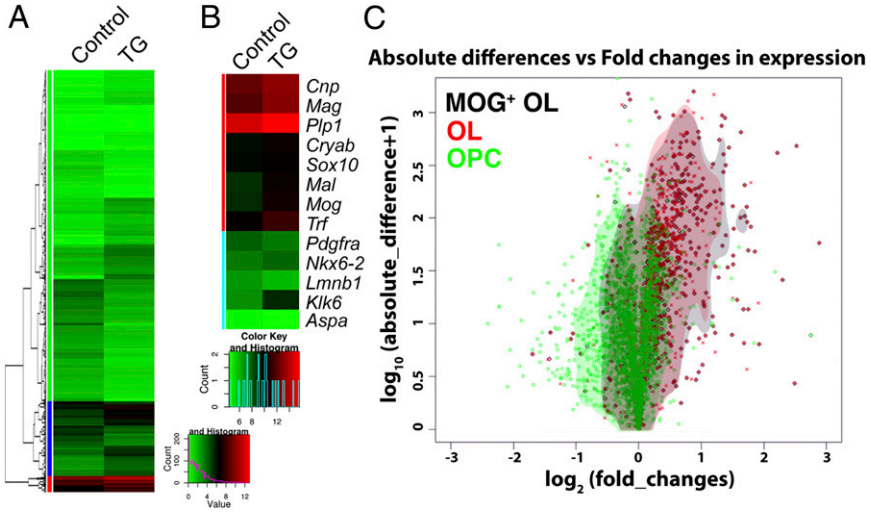

Fig. 4. Differentially expressed transcriptome in *miR-23a*–overexpressing oligodendroglia. (*A*) Hierarchical clustering and analysis of overall expressed genes in cultured OLs overexpressing *miR-23a*. (*B*) Differential expression of known myelin-associated genes plotted on a color scale (green, low expression; red, high expression). (*C*) Volcano plot and kernel density estimation demonstrate the differences in the expression patterns of genes known to be enriched at different stages of oligodendrocyte differentiation (OPC, progenitors; OL, myelinating OL; MOG^+, mature OL expressing MOG) in response to *miR-23a* overexpression.

HEK293 cells transiently coexpressing *miR-23a* and its targets. By RIP-qPCR, *PTEN* or *2700046G09Rik* coprecipitating with AGO2 was specifically enriched in *miR-23a*–transfected cells (Fig. 5*C*), indicating that *miR-23a* is facilitating AGO2 association with *PTEN* or *2700046G09Rik*. Furthermore, using a biotin-coupled *miR-23a* mimic, we observed a significant enrichment of *PTEN* or *2700046G09Rik* in *miR-23a*–captured fraction compared with control (Fig. 5*D*). Consistently, the levels of PTEN are decreased (Fig. 5*E*), whereas *2700046G09Rik* are increased (Fig. 5*F*) in spinal cord and cerebellum of *Cnp–miR-23* mice compared with WT mice. Taken together, these results strongly imply that direct interactions exist between *miR-23a* and *PTEN* or *2700046G09Rik* and that *PTEN* and *2700046G09Rik* are true *miR-23a* targets.

***2700046G09Rik* Participates in Myelin Regulation.** To understand the role of *2700046G09Rik* in oligodendroglial differentiation and myelin production, we examined its expression in various cells. RNA levels of *2700046G09Rik* were significantly higher in cultured OLs from WT mice under differentiation conditions, whereas astrocytes displayed a comparable level to cultured OPCs under proliferative conditions (Fig. S6*A*). Congruently, its level is increased in OLs from *Cnp–miR-23a* compared with WT OLs. Overexpression of *2700046G09Rik* in cultured OLs led to moderately increased expression of MAG protein (Fig. S6*B*). In addition, promoter region reporter assays revealed that two important oligodendrocyte-associated transcription factors for OPCs differentiation to OLs, YY1 and Nkx2.2 (17, 18), display positive effects on the expression of *2700046G09Rik* (Fig. 5*G*). Together, these data support a potential unique role for *2700046G09Rik* in the regulation of myelination.

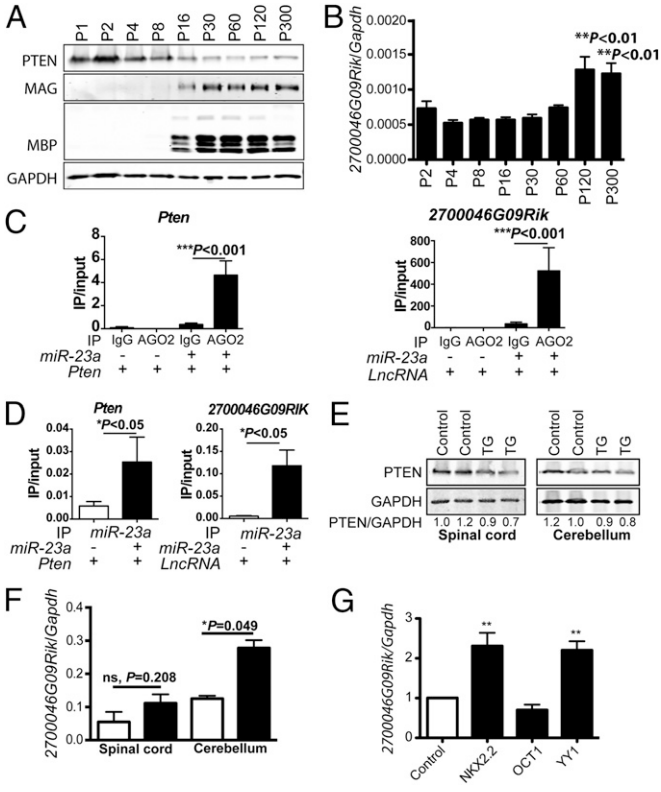

Fig. 5. *miR-23a* regulates PTEN and *2700046G09Rik*. (*A*) Western analysis of PTEN, MAG, MBP, and GAPDH from C57BL/6 brain at indicated ages. (*B*) qRT-PCR of *2700046G09Rik* from C57BL/6 brain. $^{**}P < 0.01$ compared with P0, one-way ANOVA. (*C*) Immunoprecipitation of FLAG-tagged AGO2 from HEK293 transfected with *PTEN* 3′-UTR or *2700046G09Rik* and FLAG-AGO2 plus vector or *miR-23a*. *PTEN* and *2700046G09Rik* levels were quantified by qRT-PCR, and the relative immunoprecipitate (IP)/input ratios were plotted. $n = 4$, $^{***}P < 0.001$, unpaired Student *t* test. (*D*) The 3′-end biotinylated *miR-23a* duplexes were transfected into HEK293. After streptavidin capture, input and bound fractions were evaluated by qRT-PCR. $n = 4$, $^{*}P < 0.05$. (*E*) Western analysis of PTEN in spinal cord or cerebellum from WT and *Cnp–miR-23a* mouse brain at P90. (*F*) qRT-PCR of *2700046G09Rik* transcript using spinal cord or cerebellum from control and *Cnp–miR-23a* mice. $n = 3$, $^{*}P < 0.05$. Filled bars represent *Cnp–miR-23a* and open bars denote WT mice. (*G*) Luciferase activity of firefly reporter gene fused with the 3-kb *2700046G09Rik* promoter in the presence of indicated transcription factors. $n = 4$, $^{**}P < 0.01$ compared with control, one-way ANOVA. All data are presented as ratio of means ± SEM.

Interplays Among *miR-23a*, *2700046G09Rik*, and *PTEN*. The competitive endogenous RNA hypothesis (19) suggested that coding and noncoding transcripts share common miRNA binding elements and lead to altered transcriptome homeostasis. To test whether *PTEN*, *2700046G09Rik*, and *miR-23a* have interplay in regulating OL and myelin, we first investigated the possible regulatory effects of *2700046G09Rik* on *PTEN* in cell culture. The coding region plus 2 kb 3′-UTR of *PTEN* was cotransfected into HEK293 with either *miR-23a* or *2700046G09Rik* and Western blot analysis revealed that *miR-23a* and *2700046G09Rik* both exert repressive effects on *PTEN* (Fig. 6*A*). Next, luciferase reporters carrying full-length (6 kb) 3′-UTR (20) of *PTEN* was coexpressed with *miR-23a* and/or *2700046G09Rik* (Fig. 6*B*). *2700046G09Rik* did not significantly alter the level of *PTEN*, whereas *miR-23a* displayed moderate repression. Interestingly, the level of *PTEN* was reduced by *2700046G09Rik* only in the presence of the *PTEN* coding region together with 2 kb 3′-UTR (Fig. 6 *A* and *C*). This effect was abrogated by mutating the *miR-23a* binding motif of *2700046G09Rik* (Fig. 6*C*, lane 4), suggesting that an intact *miR-23a* binding motif is necessary for the full repressive effect of *2700046G09Rik* on PTEN and that there is a possible interplay between *miR-23a* and *2700046G09Rik* for regulation of PTEN. As expected, the level of PTEN was further reduced by the presence of both *miR-23a* and *2700046G09Rik* (Fig. 6*C*, lane 5).

We next investigated the possible effect of *2700046G09Rik* and *miR-23a* on each other. Inhibition of de novo transcription by actinomycin D treatment in HEK293 cells showed *miR-23a* has a longer half-life compared with U6 small nuclear RNA (snRNA) (Fig. 6*D*). Cotransfection of *2700046G09Rik* containing perfect *miR-23a* binding elements with *miR-23a* led to higher expression of *miR-23a* in HEK293 cells following 24-h treatment of actinomycin D, whereas *miR-23a* did not alter stability of *2700046G09Rik* regardless of the presence of *miR-23a* binding elements (Fig. 6*E*). These results suggested that *2700046G09Rik* enhances *miR-23a* stability. HEK293 cells expressing *miR-23a*, *2700046G09Rik*, or both were then accessed by RIP-qPCR following immunoprecipitation of DCP1 (decapping enzyme 1) for P body (processing bodies). Coexpression of *miR-23a* and *2700046G09Rik* significantly increased *miR-23a* in DCP1 immunoprecipitant (Fig. 6*F*), indicating enrichment of *miR-23a* in P bodies by *2700046G09Rik*. Altered stability and cellular localization of *miR-23a* by *2700046G09Rik* suggest a unique role for noncoding transcripts in the regulation of *PTEN* transcript. Together, these results demonstrate a network of regulatory pathway, including *miR-23a*, *2700046G09Rik*, and PTEN in the regulation of OL development and myelin gene expression.

Signaling Pathways Modulated by *miR-23a* Overexpression. Because PTEN is a lipid phosphatase that negatively regulates the phosphatidylinositol 3-kinase (PI3K) signaling pathway (21), and accumulating evidence indicates that the PI3K/Akt/mTOR pathway regulates CNS myelination (22, 23), we investigated the possibility that *miR-23a* has a role in modulating the PI3K/Akt/mTOR signal transduction cascade. Western blot analysis revealed that the level of phosphorylated Akt was higher in *miR-23a* brain homogenate (Fig. 7*A*), indicating activation of Akt signaling. In addition, levels of PI3K signaling and MAPK activity, but not protein kinase A (PKA), were also elevated (Fig. S7 *A*–*C*). Ectopic expression of PTEN in cultured OLs purified from control and *Cnp–miR-23a* mice at P7 reduced expression levels of

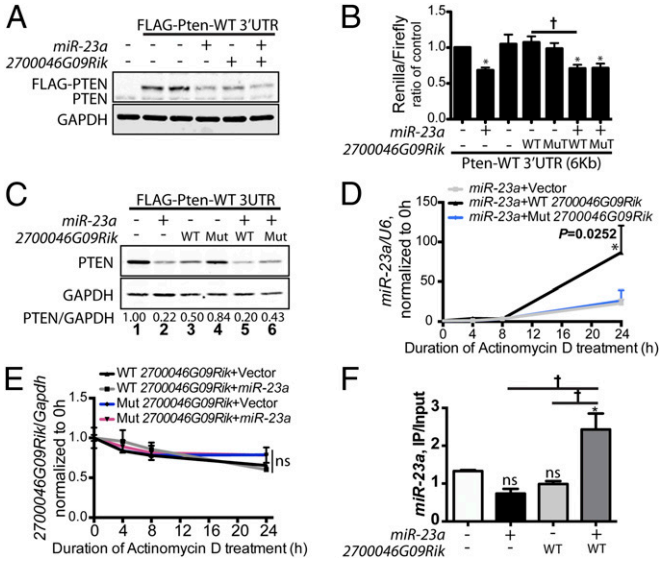

Fig. 6. *miR-23a* and *2700046G09Rik* repress PTEN. (*A*) Representative Western analysis of PTEN from HEK293 coexpressing *PTEN* coding sequences fused to 2-kb *PTEN* 3′-UTR with either *miR-23a*, *2700046G09Rik*, or both. (*B*) Luciferase activity of firefly reporter gene fused with the 6-kb full-length *PTEN* 3′-UTR (without coding region) in the presence of indicated RNA. WT, *2700046G09Rik* with normal *miR-23a* binding elements. Mut, *2700046G09Rik* with mutated *miR-23a* binding elements (M123, Fig. S5). Data presented as ratio of means ± SEM $*P < 0.05$ compared with control; $^{\dagger}P < 0.05$ compared with WT *2700046G09Rik*; one-way ANOVA. (*C*) Representative Western analysis of PTEN from HEK293 coexpressing *PTEN* coding sequences fused to 2-kb 3′-UTR (containing WT *miR-23a* binding elements) together with *miR-23a* and/or *2700046G09Rik*. (*D*) qRT-PCR analysis of *miR-23a* in HEK293 transfected with *miR-23a* plus vector (gray), *2700046G09Rik* carrying WT (black), or Mut (blue) *miR-23a* binding elements followed by actinomycin D treatment. $n = 6$, $*P < 0.05$ compared with vector control. One-way ANOVA analysis with Newman–Keuls test at 24 h. (*E*) qRT-PCR analysis of *2700046G09Rik* transcript in HEK293 transfected with *miR-23a* plus *2700046G09Rik* carrying WT (black) or Mut (blue) *miR-23a* binding elements followed by actinomycin D treatment. $n = 6$, NS, nonsignificant. (*F*) Immunoprecipitation of DCP1 from HEK293 cells transfected with vector, *miR-23a*, *2700046G09Rik*, or *miR-23a* plus *2700046G09Rik*. *miR-23a* levels were quantified by qRT-PCR, and the relative immunoprecipitate (IP)/input ratios were plotted. $n = 4$, NS, nonsignificant, $*P < 0.05$, $^{\dagger}P < 0.05$.

MAG compared with vector control (Fig. 7*B*). Overexpressing dominant-negative Akt (AKT-DN) dramatically reduced expression of myelin proteins in *Cnp–miR-23a* (Fig. 7*C*), consistent with the hypothesis that Akt acts downstream of *miR-23a* to mediate myelin formation. Rapamycin, the mTOR inhibitor, treatment reduced expression levels of several myelin proteins (PLP, MOG, and MAG) in cultured OLs isolated from *Cnp–miR-23a* mice (Fig. 7*D*). Collectively, these results confirm that PTEN/PI3K/Akt/mTOR is part of the cascade in *miR-23a*–mediated regulation and that mTOR acts downstream of *miR-23a* to mediate myelin production.

Discussion

The deposition of a precise amount of myelin around axons is necessary for proper impulse transmission, whereas too much or too little myelin surrounding axons causes nerve dysfunction in various neurological diseases. We have generated a mouse model overexpressing *miR-23a* that produces excessive myelin protein and myelin formation in the CNS. These mice display severe motor deficits beginning in postnatal life. Because *Cnp* expresses in both central and peripheral nervous systems (PNS), we cannot exclude the possibility that the motor deficits observed in *Cnp–miR-23a* mice were caused, at least in part, by peripheral myelin abnormality. Using this mouse model, we also produced a profile for differentially expressed genes that are associated with *miR-23a* overexpression. This *miR23a*-myelin transcriptome offers a useful resource for future investigation in understanding the signaling networks and factors that are required for the regulation of OL development/myelination and other *miR-23a*–regulated biological functions.

Our demonstration of *miR-23a* overexpression in OLs resulting in hypermyelination of mouse brain establishes a regulatory role for *miR-23a* in myelin production. Overexpression of *miR-23a* leads to up-regulation of genes in OL clusters, but substantial down-regulation of genes in neuronal clusters. This suggests that *miR-23a* not only functions to enhance OL lineage progression and promote myelin proteins but also safeguards against expression of genes for other cell lineages that might interfere with the progression of OL maturation and myelin sheath formation. This is consistent with previous reports that miRNAs function as guardians to enhance lineage-related protein identity and to repress other nonlineage protein expression (6, 9).

Elevated PIP3 signaling or loss of PTEN in myelinating glia has been shown to cause hypermyelination in the CNS (21, 24) and PNS (25). PTEN antagonizes PI3K signaling and negatively regulates the ERK1/2-MAPK pathway (26). Akt and mTOR, downstream effectors of PI3K signaling, promotes OL differentiation and myelin generation (22, 27, 28). Transgenic mice overexpressing constitutively active Akt kinase in OLs enhance myelin formation in the CNS but not PNS (22), and this is mediated through downstream mTOR signaling (23). The present study revealed that elevated level of *miR-23a* in OLs is sufficient to promote formation of myelin that can last until older age (at least 1-y old) partly through the Akt/mTOR and MAPK signaling pathways by targeting *PTEN*. A recent study reported that the cAMP-response element-binding protein (CREB) promotes glioma formation by up-regulating *miR-23a*, leading to down-regulation of its direct target, *PTEN* (29). Thus far, we have not observed obviously increased incidence of glioma formation in murine brains overexpressing *miR-23a* in myelinating glia.

Duplications of *LMNB1* (which encodes lamin B1) have been identified to cause adult-onset autosomal dominant leukodystrophy (30). Excessive lamin B1 expression reduces occupancy of Yin Yang 1 (YY1) transcription factor on the promoter region of PLP, thus leading to down-regulation of PLP abundance, conferring myelin loss in the mouse brain (31). Reduced levels of both PTEN and LMNB1 by *miR-23a* are likely to participate in hypermyelination observed in the present study.

To date, long noncoding RNAs have been shown to function as regulators of gene expression transcriptionally and posttranscriptionally through working at the DNA level (32), modulation of chromatin modifications, or transcriptional interference by antisense transcription (1). miRNAs bind to the coding sequences or 3′-UTRs of target transcripts, thus leading to impaired translation or increased degradation of transcripts (33). Interestingly,

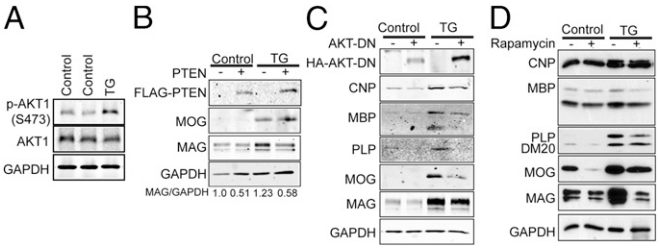

Fig. 7. *miR-23a* overexpression leads to activation of the Akt/mTOR pathway. (*A*) Western analysis of phosphor-AKT (S473) expression in corpus callosum of P90 WT or *Cnp–miR-23a* mice. (*B–D*) Representative Western analyses of myelin proteins in mouse OPCs from WT or *Cnp–miR-23a* mice cultured for 4 DIV in differentiation media. Purified OPCs were overexpressing PTEN (*B*) or dominant-negative AKT1 (AKT-DN) (*C*). (*D*) Purified OPCs were treated with 15 nM rapamycin.

2700046G09Rik, one of the *miR-23a* targets identified in this study, is a lncRNA *in cis* with the neighboring *PTEN* gene. *miR-23a* up-regulates the *2700046G09Rik* transcription, and *2700046G09Rik* in turn lengthens the half-life of *miR-23a*, thus potentiating its repressive effects. *2700046G09Rik* also can lead to a reduced level of *PTEN* expression. This down-regulation is independent of *miR-23a*–responsive elements (MREs) on *PTEN*, but requires the *miR-23a* MREs on *2700046G09Rik*. Therefore, repressive effects on PTEN can either occur with *miR-23a* alone or in coordination with *2700046G09Rik*. It is possible that *2700046G09Rik* targets the *PTEN* with the assistance of *miR-23a.* In addition, *2700046G09Rik* may aid in the cellular recompartmentation of *miR-23a* into P bodies, which could also contribute to the regulation of PTEN level. Interplay of *miR-23a* and *2700046G09Rik* in this study infers additional molecular processes in regulating mRNA decay (Fig. S8). lncRNAs are tightly controlled by environmental cues and inducible functions (34). Intriguingly, we discovered that promoter of *2700046G09Rik* can be activated by two important transcription factors (YY1 and Nkx2.2) (17, 18, 35) in OL development. Our results are consistent with a previous report that dynamic changes of lncRNA transcriptome are important for glia differentiation (36). We propose that the presence of *2700046G09Rik* in oligodendroglia potentiates and signals the activation of the *miR-23a*/PTEN/Akt/mTOR and MAPK cascades in the correct developmental stage, thus regulating the expression of myelin genes in OLs.

Noncoding RNAs (ncRNAs) have emerged as a major component in epigenetic regulation, specifically in orchestrating neural gene expression and function and gene–environment interactions (2, 37). Elevated levels of *miR-23a* are identified in severe demyelinated regions of brains derived from the murine model of autosomal dominant adult-onset leukodystrophy (Fig. S9) and active multiple sclerosis lesions in human brains (38, 39). Interestingly, increased frequency of *miR-23a* rs(refSNP) 3745453 C allele has been identified as a potential risk factor of multiple sclerosis (39). Therefore, *miR-23a* may participate in not only modulating genes in normal myelin regulation but also in myelin repair. Through identification of *miR-23a* targets, we revealed that *miR-23a* and some lncRNAs (*2700046G09Rik*) interact in a complex regulatory network to modulate genes that are important for myelin formation/maintenance. Understanding the layers of complexity in the molecular mechanisms that underlie the elaboration of myelin synthesis and maintenance has undergone intensive investigation and recent advances have uncovered unique insights into these processes. Identifying targets of *miR-23a* and developing future demyelinating experiments using this murine model will provide the opportunity to better understand RNA regulatory networks and offer future therapeutic approaches against demyelinating diseases.

Materials and Methods

Details for generation of *Cnp–miR-23a* mice oligodendrocyte culture, RNA-Seq analysis, immunoblotting, immunostaining, and qRT-PCR are provided in *SI Materials and Methods*. *Cnp-miR-23a* mice were generated and maintained in C57BL/6 background. All animal experiments were performed under approval by the Animal Care and Use Committee at the University of California, San Francisco.

ACKNOWLEDGMENTS. We acknowledge V. Gallo for the *Cnp*-promoter constructs; M. Kato for the *PTEN*-luciferase construct; Y. Zhao, L.-Y. Hsu, H.-E. Liang, and J. Pollack for suggestions in mouse generation and statistical analysis; D. H. Rowitch and J. R. Chan for helpful discussions; and B. Barres for implementing primary culturing methods, S.-Y. C. Chong for editing the manuscript, and members of the Y.-H.F. and L.J.P. laboratories for discussions. This work was supported by National Institutes of Health Grant NS062733 (to Y.-H.F.) and the Sandler Neurogenetics Fund (Y.-H.F. and L.J.P.). L.J.P. is an Investigator of the Howard Hughes Medical Institute.

1. Pauli A, Rinn JL, Schier AF (2011) Non-coding RNAs as regulators of embryogenesis. *Nat Rev Genet* 12(2):136–149.
2. Qureshi IA, Mehler MF (2012) Emerging roles of non-coding RNAs in brain evolution, development, plasticity and disease. *Nat Rev Neurosci* 13(8):528–541.
3. Lewis BP, Burge CB, Bartel DP (2005) Conserved seed pairing, often flanked by adenosines, indicates that thousands of human genes are microRNA targets. *Cell* 120(1):15–20.
4. Xu N, Papagiannakopoulos T, Pan G, Thomson JA, Kosik KS (2009) MicroRNA-145 regulates OCT4, SOX2, and KLF4 and represses pluripotency in human embryonic stem cells. *Cell* 137(4):647–658.
5. Cheng LC, Pastrana E, Tavazoie M, Doetsch F (2009) miR-124 regulates adult neurogenesis in the subventricular zone stem cell niche. *Nat Neurosci* 12(4):399–408.
6. Lau P, et al. (2008) Identification of dynamically regulated microRNA and mRNA networks in developing oligodendrocytes. *J Neurosci* 28(45):11720–11730.
7. Budde H, et al. (2010) Control of oligodendroglial cell number by the miR-17-92 cluster. *Development* 137(13):2127–2132.
8. Dugas JC, et al. (2010) Dicer1 and miR-219 are required for normal oligodendrocyte differentiation and myelination. *Neuron* 65(5):597–611.
9. Zhao X, et al. (2010) MicroRNA-mediated control of oligodendrocyte differentiation. *Neuron* 65(5):612–626.
10. Shin S, et al. (2009) MicroRNAs are significantly influenced by p53 and radiation in HCT116 human colon carcinoma cells. *Int J Oncol* 34(6):1645–1652.
11. Lin ST, Fu YH (2009) miR-23 regulation of lamin B1 is crucial for oligodendrocyte development and myelination. *Dis Model Mech* 2(3–4):178–188.
12. Belachew S, Yuan X, Gallo V (2001) Unraveling oligodendrocyte origin and function by cell-specific transgenesis. *Dev Neurosci* 23(4–5):287–298.
13. Hu X, et al. (2006) Bace1 modulates myelination in the central and peripheral nervous system. *Nat Neurosci* 9(12):1520–1525.
14. Cahoy JD, et al. (2008) A transcriptome database for astrocytes, neurons, and oligodendrocytes: A new resource for understanding brain development and function. *J Neurosci* 28(1):264–278.
15. Rinn JL, Chang HY (2012) Genome regulation by long noncoding RNAs. *Annu Rev Biochem* 81:145–166.
16. Chi SW, Zang JB, Mele A, Darnell RB (2009) Argonaute HITS-CLIP decodes microRNA-mRNA interaction maps. *Nature* 460(7254):479–486.
17. He Y, et al. (2007) The transcription factor Yin Yang 1 is essential for oligodendrocyte progenitor differentiation. *Neuron* 55(2):217–230.
18. Qi Y, et al. (2001) Control of oligodendrocyte differentiation by the Nkx2.2 homeodomain transcription factor. *Development* 128(14):2723–2733.
19. Salmena L, Poliseno L, Tay Y, Kats L, Pandolfi PP (2011) A ceRNA hypothesis: The Rosetta Stone of a hidden RNA language? *Cell* 146(3):353–358.
20. Kato M, et al. (2009) TGF-beta activates Akt kinase through a microRNA-dependent amplifying circuit targeting PTEN. *Nat Cell Biol* 11(7):881–889.
21. Goebbels S, et al. (2010) Elevated phosphatidylinositol 3,4,5-trisphosphate in glia triggers cell-autonomous membrane wrapping and myelination. *J Neurosci* 30(26):8953–8964.
22. Flores AI, et al. (2008) Constitutively active Akt induces enhanced myelination in the CNS. *J Neurosci* 28(28):7174–7183.
23. Narayanan SP, Flores AI, Wang F, Macklin WB (2009) Akt signals through the mammalian target of rapamycin pathway to regulate CNS myelination. *J Neurosci* 29(21):6860–6870.
24. Harrington EP, et al. (2010) Oligodendrocyte PTEN is required for myelin and axonal integrity, not remyelination. *Ann Neurol* 68(5):703–716.
25. Goebbels S, et al. (2012) Genetic disruption of Pten in a novel mouse model of tomaculous neuropathy. *EMBO Mol Med* 4(6):486–499.
26. Pezzolesi MG, Zbuk KM, Waite KA, Eng C (2007) Comparative genomic and functional analyses reveal a novel cis-acting PTEN regulatory element as a highly conserved functional E-box motif deleted in Cowden syndrome. *Hum Mol Genet* 16(9):1058–1071.
27. Barros CS, et al. (2009) Beta1 integrins are required for normal CNS myelination and promote AKT-dependent myelin outgrowth. *Development* 136(16):2717–2724.
28. Tyler WA, et al. (2009) Activation of the mammalian target of rapamycin (mTOR) is essential for oligodendrocyte differentiation. *J Neurosci* 29(19):6367–6378.
29. Tan X, et al. (2012) cAMP response element-binding protein promotes gliomagenesis by modulating the expression of oncogenic microRNA-23a. *Proc Natl Acad Sci USA* 109(39):15805–15810.
30. Padiath QS, et al. (2006) Lamin B1 duplications cause autosomal dominant leukodystrophy. *Nat Genet* 38(10):1114–1123.
31. Heng MY, et al. (2013) Lamin B1 mediates cell-autonomous neuropathology in a leukodystrophy mouse model. *J Clin Invest* 123(6):2719–2729.
32. Ørom UA, et al. (2010) Long noncoding RNAs with enhancer-like function in human cells. *Cell* 143(1):46–58.
33. Bartels CL, Tsongalis GJ (2009) MicroRNAs: Novel biomarkers for human cancer. *Clin Chem* 55(4):623–631.
34. Geisler S, Lojek L, Khalil AM, Baker KE, Coller J (2012) Decapping of long noncoding RNAs regulates inducible genes. *Mol Cell* 45(3):279–291.
35. Berndt JA, Kim JG, Tosic M, Kim C, Hudson LD (2001) The transcriptional regulator Yin Yang 1 activates the myelin PLP gene. *J Neurochem* 77(3):935–942.
36. Mercer TR, et al. (2010) Long noncoding RNAs in neuronal-glial fate specification and oligodendrocyte lineage maturation. *BMC Neurosci* 11:14.
37. Wang KC, Chang HY (2011) Molecular mechanisms of long noncoding RNAs. *Mol Cell* 43(6):904–914.
38. Junker A, et al. (2009) MicroRNA profiling of multiple sclerosis lesions identifies modulators of the regulatory protein CD47. *Brain* 132(Pt 12):3342–3352.
39. Ridolfi E, et al. (2013) Expression and genetic analysis of microRNAs involved in multiple sclerosis. *Int J Mol Sci* 14(3):4375–4384.

Supporting Information

Lin et al. 10.1073/pnas.1317182110

SI Materials and Methods

Generation of *Cnp–miR-23a* Mice. We generated transgenic mice overexpressing microRNA-23a (miR-23a) driven by the *Cnp* promoter (1). To selectively overexpress *miR-23a* among the *miR-23a–miR-27a–miR-24–2* cluster, various *miR-23a* flanking sequences were expressed in HEK293 cells. Northern blotting revealed that the strongest expression of *miR-23a* transgene occurred when the pre–*miR-23a* was flanked on each side with 120-nt genomic sequences (Fig. S2*B*). The 120-nt flanking sequences only included partial pre–*miR-27a*; therefore, it did not result in overexpression of *miR-27a* and *miR-24–2*. This mouse genomic fragment was further subcloned into an expression vector downstream of a murine *Cnp* promoter for generating transgenic animal (Fig. S2*C*). The pre–*miR-23a* plus 120-bp flanking sequences on each side was inserted downstream of *Cnp1* and *Cnp2* promoters and the construct was used to generate transgenic C57BL/6 mice at the University of California, San Francisco (UCSF) mouse transgenic core. Positive founders were identified by PCR amplification of tail DNA using Cnp F (5′-GCCCCAGGCCTCCAAACAGGACAT) and miR-23a R (5′-GACCTTGCTCACAAGCAGCTAAG). *miR-23a* expressed in oligodendrocytes in the CNS was noted in all seven lines. For simplicity and consistency, *Cnp–miR-23a*-H was used for follow-up analyses. A notable unilateral hindlimb paralysis in *Cnp–miR-23a* mice was found in ∼25% of transgenic mice derived from intercrossing middle and high expressing lines of *Cnp–miR-23a*. All mouse experiments were performed in compliance with animal protocols approved by the Animal Care and Use Committee at UCSF.

Behavioral Examination. All behavioral evaluations were performed in the morning between the hours of 9:00 AM and noon.

Balance beam. Motor coordination, balance, and hindlimb placement were evaluated by assessing the ability of mice to transverse two types of balance beams to reach an enclosed safety platform. Each mouse was tested for its ability to transverse different styles of 41-cm-long scored Plexiglas beams (2). Two square (5 mm and 11 mm) beams were used in this study. Beams were placed horizontally 50 cm above a table. A brightly illuminated start platform and a darkened enclosed 80,000 cm^3 escape box (20 × 20 × 20 cm) were situated at the end of the beam. Time to traverse each beam was recorded for each trail with a 20-s maximum cutoff, and falls were scored at 20 s. The number of foot slips and whether a mouse dragged itself across the beam on its abdomen was also recorded.

Horizontal wire hang test. A standard wire cage lid is used with masking tape placed around the perimeter of the lid to prevent animals from escaping. After an animal is placed in the lid, the lid is shaken gently to induce a firm grip, and the lid is inverted. The lid is held horizontally 20 cm above the cage litter. Latency to fall is recorded for up to 2 min (3).

Coat hanger test. Mice are placed in the middle of a thin horizontal bar (2 mm diameter; 40 cm length; 85 cm higher from a blanket-covered table), in an upside-down position. The time taken for the mice to travel along the bar of the triangular-shaped coat hanger was recorded together with the latencies to fall with a cutoff point of 2 min.

Histology and Immunostaining. Mice were anesthetized with avertin and perfused through the left ventricle with PBS followed by 4% (wt/vol) paraformaldehyde in PBS. Brains and spinal cords were postfixed overnight at 4°and cryostated. Coronal section (15 μm) were incubated overnight at 4° in primary antibody followed by 1 h at room temperature with the corresponding fluorescently labeled secondary antibodies conjugated to either Alexafluor 495 or Alexafluor 594 (1:500; Invitrogen) and analyzed as described previously (4). Myelinated fibers were visualized by Luxol Fast Blue (Sigma) staining.

Cell Culture, Transfection, and Immunocytochemistry. HEK293 cells were cultured as described previously (4). Primary glial cultures were isolated from adult *Cnp–miR-23a* overexpressing transgenic mice or WT littermates using standard methods (5). Plasmid or single-stranded RNA transfections (Dharmacon) were performed by using FuGene HD (Roche) or nucleofector electroporation with the Amaxa system (Amaxa Biosystems). Cells grown on coverslips were fixed in methanol at −20 °C or 4% (wt/vol) paraformaldehyde in PBS at room temperature. Immunocytochemistry was performed as described previously (4).

Luciferase Reporter Assay. Luciferase activities in the cell extracts were assayed 48 h after transfection as described previously (4). pGL3-promoter expression constructs were cotransfected to normalize for transfection efficiency. pSV-RL-Luc (Promega) was used to place 3′-UTR downstream of a Renilla luciferase in this study.

Transmission Electron Microscopy and G-Ratio Analysis. Six-month-old animals were deeply anesthetized and intracardially perfused with 1% paraformaldehyde, 2% (vol/vol) glutaraldehyde in 0.1 M sodium cacodylate buffer, pH 7.4 ($n = 2$ per group for TG^+/WT, TG^+/TG^+ *Cnp–miR-23a*, and wild-type mice). Brains were postfixed in 2% (wt/vol) osmium tetroxide in the same buffer, en block stained in 2% (wt/vol) aqueous uranyl acetate, dehydrated, infiltrated, and embedded in LX-112 resin (Ladd Research Industries). Semithin sections of corpus callosum were stained with toluidine blue for tissue identification. Methods were performed as previously described with the above modifications (6). Images were collected using the Tecnai electron microscope at the UCSF EM facility.

G ratio of axons in the area of interest was obtained as a ratio of the diameter of an axon over the diameter of the axon plus associated myelin sheath. Approximately 150–200 axons per animal for each group of two animals were used. Digitized and calibrated images were analyzed using ImageJ (National Institutes of Health).

RNA Extraction, Quantitative RT-PCR, and UV–Cross-Link RIP. Total RNA from WT and *Cnp–miR-23a* brain tissues were isolated using the RNeasy Mini kit according to the manufacturer's instructions (Qiagen). For RNA-sequencing (RNA-Seq) analysis, we isolated OLs from *Cnp–miR-23a* and WT mice at P7 using established immunopanning methods (5), and three independent preparations of OLs were pooled for RNA-Seq analysis. Total RNA was collected from purified mouse OPCs cultured for 4 d in vitro (DIV) in +PDGF −T3 media followed by 4 DIV in −PDGF +T3 media. Total RNA samples (10 μg, size >200 nt) isolated using the Qiagen RNeasy Mini kit were pooled from three independent preparations. RNA purity was assessed using the ND-1000 Nanodrop Spectrophotometer (NanoDrop). Each RNA sample had an A260:A280 ratio above 1.8 and A260:A230 ratio above 2.0. cDNA was generated from total RNA (2 μg) by SuperScript III first-strand synthesis system (Invitrogen) and transcripts were detected and amplified by quantitative real-time PCR in a RotorGene RG3000 real-time PCR system (Corbett

Research) with the FastStart SYBR-green-containing master (Rox) PCR kit (Roche). UV–cross-link RIP was performed as described (7).

RNA-Seq Analysis. RNA-Seq was carried out at Active Motif (www.activemotif.com). The sequencing results were paired-end 36-bp reads shipped in FASTQ format. We used an analysis pipeline composed of commonly used software, including Bowtie (8), TopHat (9), Samtools (10), and Cufflinks (11) to align and assemble the short reads. We used a "reference based" approach, in which the alignment and assembly were based on the reference mouse genome sequence (assembly mm9 from UCSC) and the ENSEMBL annotation of mouse genes (NCBIM37.61). Briefly, we first used samstats (samstats.sourceforge.net) to examine the quality of the RNA-Seq reads. The reads were then aligned to the mouse genome using the splice-aware aligner TopHat, which used Bowtie for short read alignments. The aligned reads were sorted and indexed using Samtools. We then used Cufflinks to assemble the reads into transcripts, which converted the read coverage into the fragments per kilobases of transcripts per million fragments mapped (FPKM) metric of expression. The Cufflinks also came with Cuffcompare and Cuffdiff for unifying the names of the assembled transcripts and the expression levels among different RNA-Seq samples were compared.

Absolute difference, fold change plot, and kernel density estimation. The fold changes (FCs) ($\log_2$ of the FCs in FPKM) between wild-type (control) and *Cnp–miR-23a* and absolute differences (AD) ($\log_{10}$ of the absolute differences in FPKM) values were calculated for each gene based on the RNA-Seq results. Data points of genes in a defined gene set such as the genes overexpressed in neurons are plotted with FC as the x axis and AD as the y axis. Distribution of the genes in the plot indicated whether the genes were significantly up-regulated (toward the upper-right corner) or down-regulated (toward the upper-left corner). Distribution density of the data was estimated using the kernel density estimation method from R (www.R-project.org). Based on the estimated density and a cutoff value of 95%, control lines were drawn that encircle the colored areas in plots. These colored areas allow us to visualize the distribution of the data points. By the definition of density, with greater than 95% chances, any data point from the correspondent gene set should fall inside the colored area. The density plots of different gene sets, such as the genes are clustered in neurons, oligodendrocytes, astrocytes or oligodendrocytes at different developmental stages, are superimposed together to visualize the differences among these gene sets in the wake of aberrant expression of *miR-23a*.

MicroRNA target prediction. MicroRNA (miRNA) targets were predicted from two sources. First, we retrieved 3′-UTR of all mouse genes from ENSEMBL via BioMart and predicted the targets using Miranda (www.microrna.org/microrna/home.do) (12). We scanned for the targets that have strict seed pairing. Besides that, the default parameters of Miranda were used. The same analysis was also carried out for mouse long noncoding RNAs (lncRNAs) annotated in ENSEMBL, where the targets were predicted along the whole sequence of the lncRNAs. We used the target prediction from TargetScan (www.targetscan.org/mmu_50/) (13) as the second source. We retrieved the aligned 3′-UTR sequence from TargetScan and kept only the sequences from human, chimpanzee, dog, and mouse. The targets were then scanned using the targetscan_50.pl script from TargetScan. The resulting sets of targets were conserved in the four mammal species. The target information was mapped back to the transcripts and formed a combined set of data with both expression and target information.

Comparing with other transcriptome data. We compared our RNA-Seq result with the available transcriptome data for astrocytes, neurons, and oligodendrocytes (14). We retrieved the cell-type–enriched genes and mapped them to our RNA-Seq data and then plotted the absolute differences versus the FCs between gene expression in oligodendrocytes from *Cnp–miR-23a* transgenic mice and control mice.

Multidimensional scaling analysis. Multidimensional scaling (MDS) (15) is carried out to visualize the dissimilarities in expression changes among genes of neuron, astrocyte, or oligodendrocyte categories. Genes from these categories are pooled together and differentially colored. The $\log_2$ of FCs in expression between *Cnp–miR-23a* and control is calculated for each gene and the Manhattan distances in $\log_2$ of FC are calculated for all gene pairs. Two-dimension MDS is carried out on the distance matrix using the classical (metric) MDS method from the R programming language. The axes of the plot are converted coordinates from the distances that are optimized in the MDS process to recapitulate the distances among thousand of genes in a 2D space. From the plot, there is obvious clustering of genes in different categories, suggesting that genes in different categories are differently influenced by aberrant *miR-23a* expression.

Statistical Analysis. Data were presented as mean ± SEM and data comparison was undertaken using the two-tailed independent Student t test or two-way ANOVA followed by one-way ANOVA with Newman–Keuls post hoc test (Prism5; GraphPad). The significant difference was set at $P < 0.05$, unless otherwise stated. For differential expression analysis of RNA-seq data, the significant difference was set at $P \leq 0.013$ at a Benjamini–Hochberg (16) adjusted false discovery rate less than 0.05 by pairwise sample comparison using Cuffdiff and FC cutoff was set at 1.5.

1. Yuan X, et al. (2002) Expression of the green fluorescent protein in the oligodendrocyte lineage: A transgenic mouse for developmental and physiological studies. *J Neurosci Res* 70(4):529–545.
2. Heng MY, Tallaksen-Greene SJ, Detloff PJ, Albin RL (2007) Longitudinal evaluation of the Hdh(CAG)150 knock-in murine model of Huntington's disease. *J Neurosci* 27(34): 8989–8998.
3. Crawley (2000) *What's wrong with my mouse? Behavioral phenotyping of transgenic and knockout mice* (Wiley, New York).
4. Lin ST, Fu YH (2009) miR-23 regulation of lamin B1 is crucial for oligodendrocyte development and myelination. *Dis Model Mech* 2(3–4):178–188.
5. Dugas JC, Tai YC, Speed TP, Ngai J, Barres BA (2006) Functional genomic analysis of oligodendrocyte differentiation. *J Neurosci* 26(43):10967–10983.
6. Harrington EP, et al. (2010) Oligodendrocyte PTEN is required for myelin and axonal integrity, not remyelination. *Ann Neurol* 68(5):703–716.
7. Zhao J, et al. (2010) Genome-wide identification of polycomb-associated RNAs by RIP-seq. *Mol Cell* 40(6):939–953.
8. Langmead B, Trapnell C, Pop M, Salzberg SL (2009) Ultrafast and memory-efficient alignment of short DNA sequences to the human genome. *Genome Biol* 10(3):R25.
9. Trapnell C, Pachter L, Salzberg SL (2009) TopHat: Discovering splice junctions with RNA-Seq. *Bioinformatics* 25(9):1105–1111.
10. Li H, et al.; 1000 Genome Project Data Processing Subgroup (2009) The Sequence Alignment/Map format and SAMtools. *Bioinformatics* 25(16):2078–2079.
11. Trapnell C, et al. (2010) Transcript assembly and quantification by RNA-Seq reveals unannotated transcripts and isoform switching during cell differentiation. *Nat Biotechnol* 28(5):511–515.
12. John B, et al. (2004) Human MicroRNA targets. *PLoS Biol* 2(11):e363.
13. Lewis BP, Burge CB, Bartel DP (2005) Conserved seed pairing, often flanked by adenosines, indicates that thousands of human genes are microRNA targets. *Cell* 120(1):15–20.
14. Cahoy JD, et al. (2008) A transcriptome database for astrocytes, neurons, and oligodendrocytes: A new resource for understanding brain development and function. *J Neurosci* 28(1):264–278.
15. Quinn GP, Keough MJ (2002) *Experimental Design and Data Analysis for Biologists* (Cambridge Univ Press, Cambridge, UK).
16. Benjamini Y, Hochberg Y (1995) Controlling the false discovery rate: a practical and powerful approach to multiple testing. *J Roy Stat Soc B* 57:289–00.

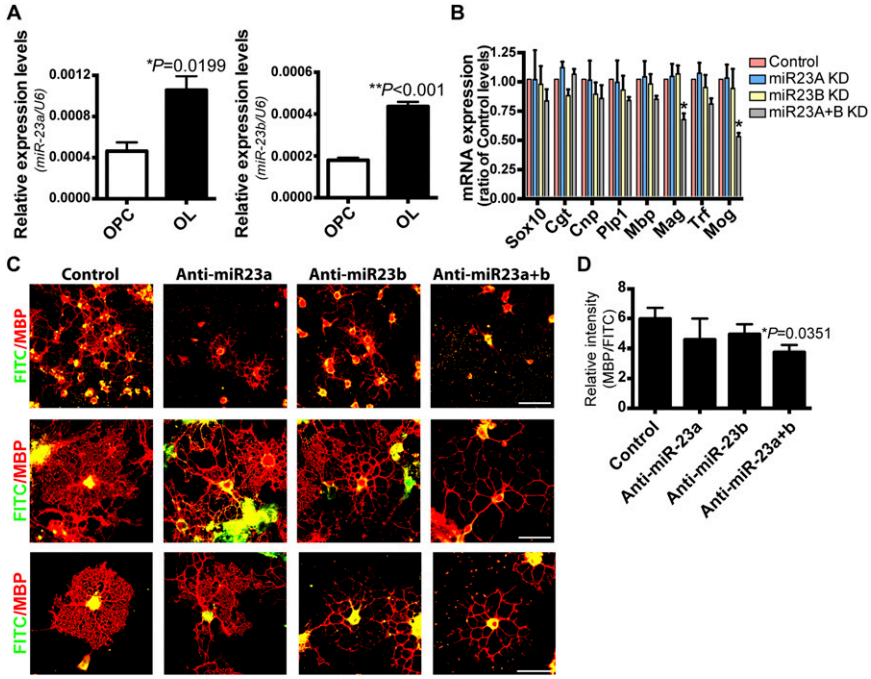

Fig. S1. *miR-23a* tightly regulates differentiation status of OLs. (*A*) Quantitative RT-PCR (qRT-PCR) of *miR-23a* and *miR*-23b in OPCs isolated from C57BL/6 mice under proliferative (OPC, open bars) or differentiation (OL, filled bars) conditions. Data are presented as ratio of means ± SEM, $n = 4$, $^{*}P < 0.05$, $^{**}P < 0.01$, unpaired Student *t* test. (*B*) Expression levels of myelin genes in cultured OPCs containing antagomirs knocking down *miR-23a*, *miR-23b*, or *miR-23a*+*miR-23b* in differentiation conditions for 4 d. Data are presented as ratio of means ± SEM, $n = 3$, $^{*}P < 0.05$, one-way ANOVA with Newman–Keuls post hoc test. (*C*) Representative images of OPCs transfected with FITC-labeled antagomirs against *miR-23a*, *miR-23b*, or *miR-23a*+*miR-23b* and differentiated for 4 d before stained with MBP. [Scale bar, 50 μm (*Top*) or 10 μm (*Middle* and *Bottom*)]. (*D*) Quantification of MBP immunoreactivity in OPCs transfected with FITC-labeled antagomirs against *miR-23a*, *miR-23b*, or *miR-23a*+*miR-23b* and differentiated for 4 d. Data are presented as ratio of MBP/FITC in FITC-labeled cells from three independent experiments. $n = 4$, $^{*}P < 0.05$, One-way ANOVA with Newman–Keuls post hoc test.

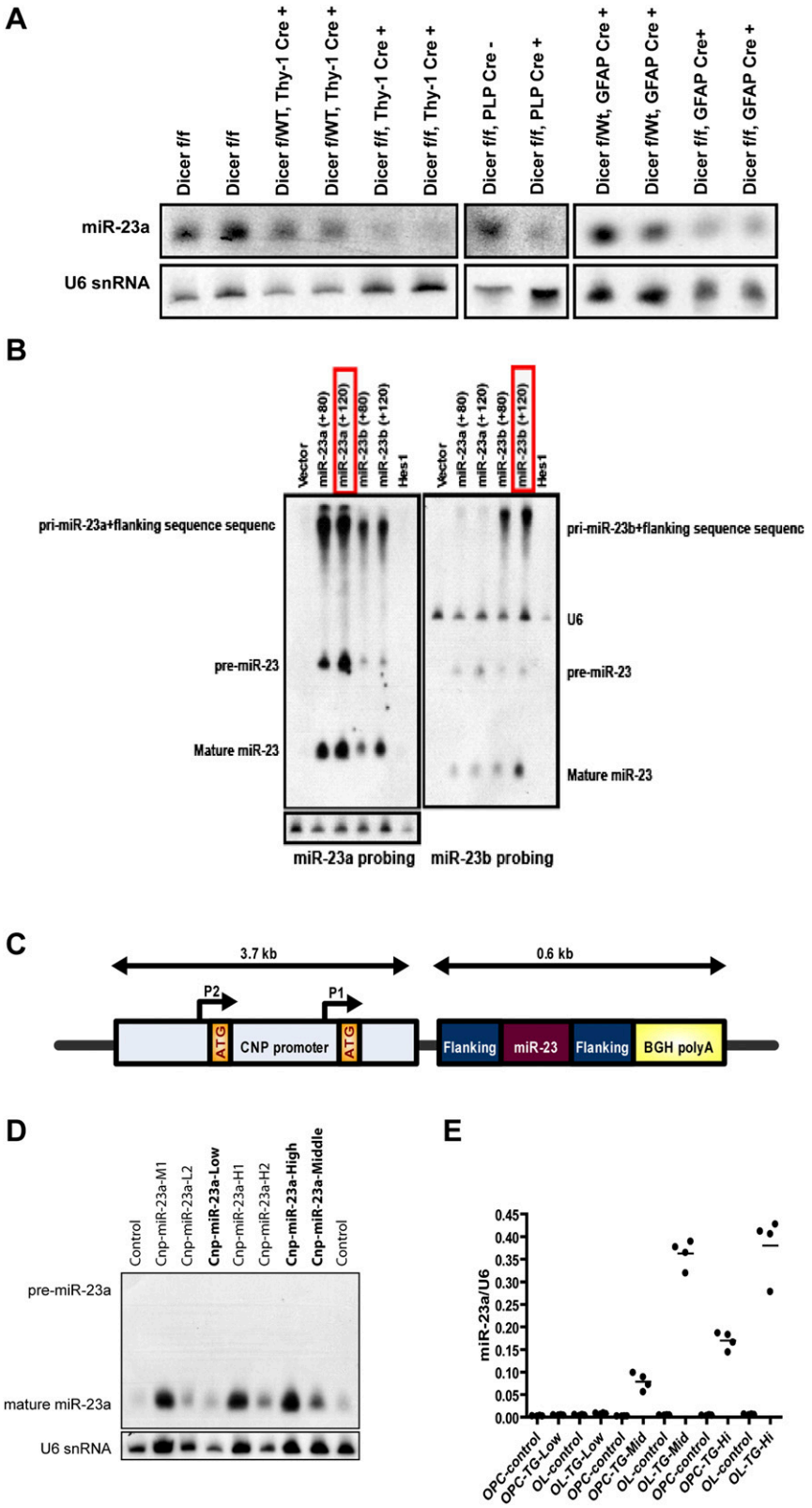

Fig. S2. (*A*) Northern blot analysis of RNA isolated from *Dicer*-ablated mouse brain of indicated lineage: Thy-1 for neurons, PLP for OLs, and GFAP for astrocytes. (*B*) Northern blot analysis of *miR-23a* transgene with various lengths of flanking sequences in HEK293 cells. The probes used were *miR-23a*, *miR-23b*, and *U6* small nuclear (sn)RNA. (*C*) Schematic diagram of the *Cnp–miR-23a* construct used in transgenic mouse generation. (*D* and *E*) Whole brain samples (*D*) or cultured oligodendroglia (*E*) from WT and *Cnp–miR-23a* mice were analyzed for *miR-23a* expression by Northern blot or qRT-PCR of *miR-23a*.

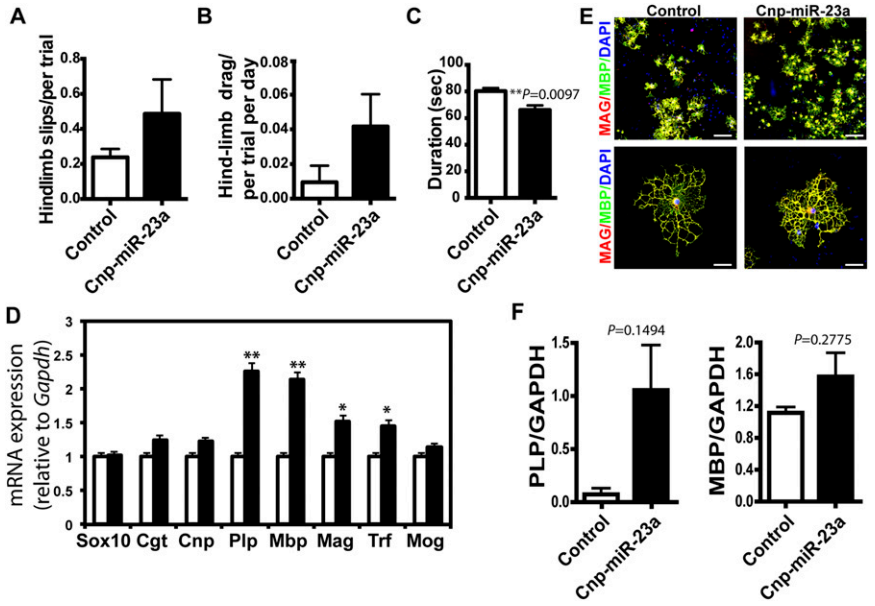

Fig. S3. (*A*) Number of hindlimb footslips, and (*B*) rate of hindlimb dragging while traversing a 5-mm square balance beam. (*C*) Measurement of time for *Cnp–miR-23a* mice to stay on the coat hanger. Filled bars represent *Cnp–miR-23a* and open bars denote WT mice. Data are presented as ratio of means ± SEM, $n = 7$ per genotype, $^{**}P < 0.01$, unpaired Student *t* test. (*D*) Expression of OL markers in cells purified from P7 WT and *Cnp–miR-23a* mice cultured in proliferation medium followed by qRT-PCR. Data are presented as ratio of means ± SEM, normalized to control, $^{*}P < 0.05$, $^{**}P < 0.01$, unpaired Student *t* test. $n = 4$ per genotype. Filled bars represent *Cnp–miR-23a* OPCs and open bars denote WT OPCs. (*E*) OPCs purified from P7 WT and *Cnp–miR-23a* mice cultured for 4 d in vitro (DIV) in differentiation medium followed by staining for MBP (green), MAG (red), and DAPI (blue). (Scale bar, 50 μm or 10 μm.) (*F*) Quantitation of Western blot analyses showed increased expression of PLP and MBP in *Cnp–miR-23a* OLs relative to control. Protein lysates were purified from OPCs cultured at 4 DIV in differentiation media. GAPDH was used as a loading control. Data were obtained from three independent experiments.

A

Top 5 canonical functions using IPA of genes in *miR-23a* overexpressing oligodendrocytes		
	No. of molecules	*P* values
Organism survival	847	1.02E-29~7.43E-07
Nervous system development and function	1382	1.03E-26~8.16E-07
Organism development	928	4.31E-20~8.02E-07
Connective tissue development and function	410	4.34E-14~2.69E-07
Tissue development	833	3.43E-13~8.90E-07

B

Top 5 canonical functions using IPA of genes that are downregulated in *miR-23a* overexpressing oligodendrocytes		
	No. of molecules	*P* values
Glutamate receptor signaling	8	2.75E-06
ERK/MAPK signaling	10	6.54E-04
Clathrin-mediated endocytosis signaling	9	9.07E-04
Caveolar-mediated endocytosis signaling	6	9.82E-04
Neuropathic pain signaling in dorsal horn neurons	7	9.85E-04

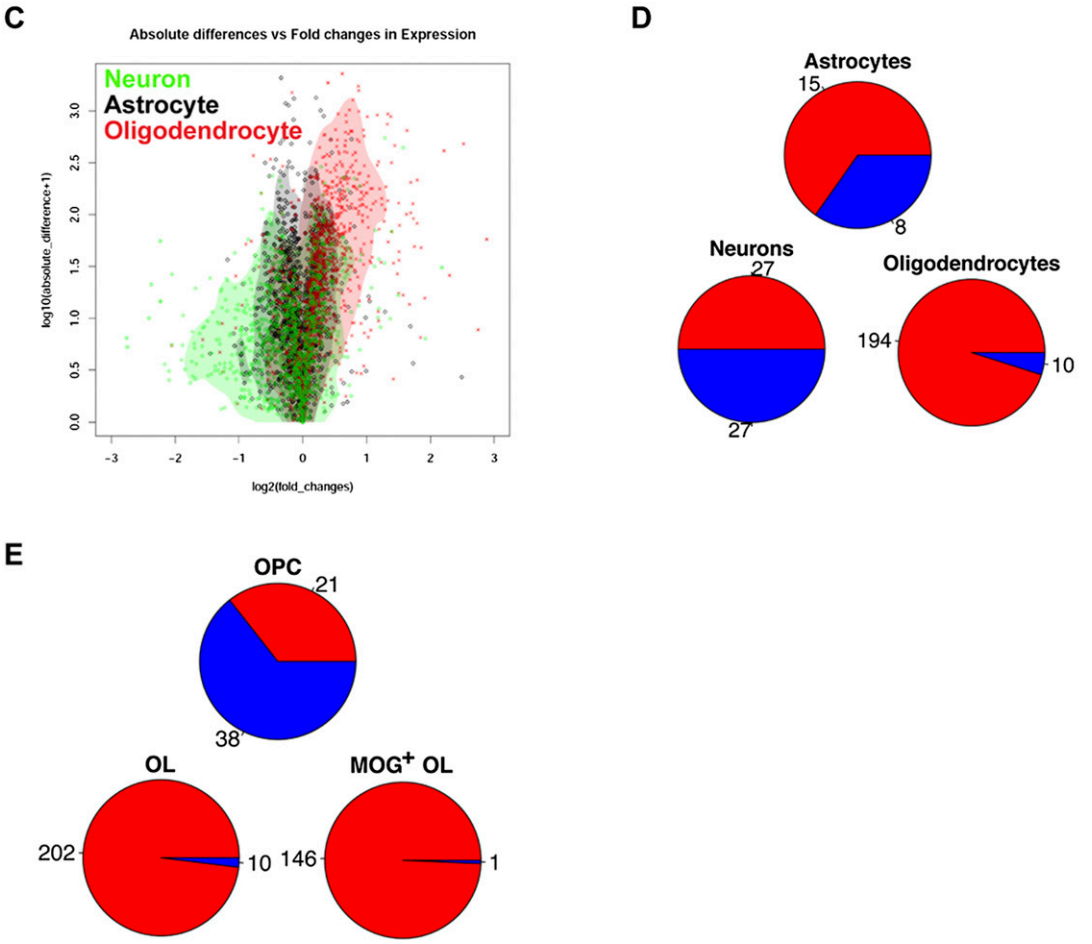

Fig. S4. Differential transcriptomes of OLs overexpressing *miR-23a*. (*A*) Top five physiological functions identified using Ingenuity pathway analysis (IPA) of total genes. (*B*) Top five canonical functions containing differentially down-regulated genes identified by using IPA. (*C*) Differentially expressed genes enriched in neurons (green), astrocytes (black), or OLs (red). (*D*) Pie diagram of significantly differentially expressed genes (absolute FC ≥1.5) clustered in neurons, astrocytes, or OLs. (*E*) Pie diagram of significantly differentially expressed genes (absolute FC ≥1.5) enriched in oligodendrocyte progenitors (OPC), myelinating OLs (OL), or the most mature OLs with MOG expression (MOG^+ OL). Red indicates up-regulation and blue indicates down-regulation for (*D* and *E*).

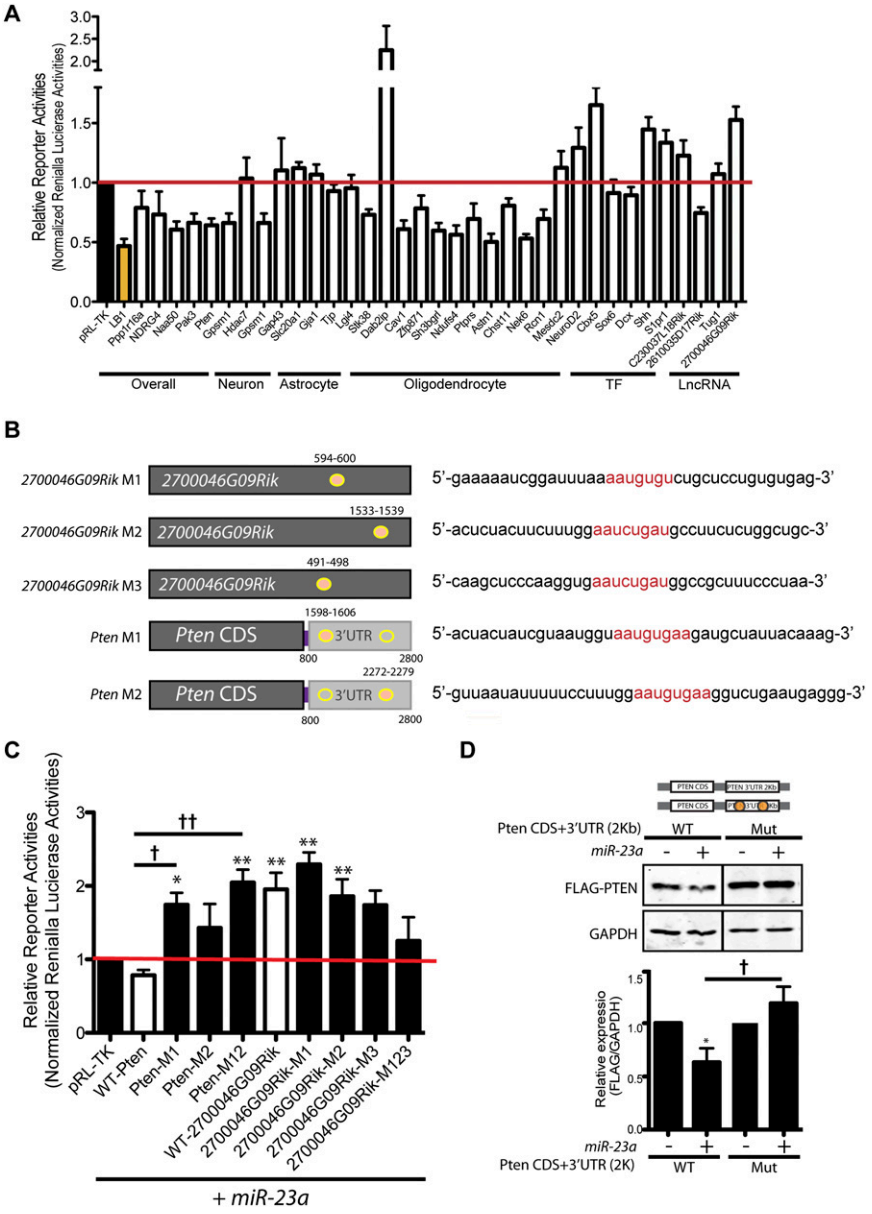

Fig. S5. *miR-23a* regulates *PTEN* and *2700046G09Rik*. (*A*) Luciferase activity assay in HEK293 overexpressing *miR-23a* and luciferase constructs carrying additional 3′-UTR of targeting candidates. Filled bar denotes luciferase coding sequence without additional 3′-UTR; orange filled bar indicates luciferase with additional *Lmnb1* 3′-UTR as a positive control. Data represent means ± SEM, $n = 4$. TF, transcription factor. (*B*) Regions of the *PTEN* and *2700046G09Rik* 3′-UTR with mutated *miR-23a*–responsive elements (MREs predicted by the TargeScan and miRANDA, in red) were cloned into the luciferase reporter constructs as depicted. (*C*) Luciferase activity in HEK293 cotransfected with *miR-23a* and reporter constructs containing WT or mutated *miR-23a* binding sites. Data represent means ± SEM, $n = 4$, and normalized to the control. $^{*}P < 0.05$, $^{**}P < 0.01$ compared with control group; $^{\dagger}P < 0.05$, $^{\dagger\dagger}P < 0.01$ compared with WT. One-way ANOVA with Newman–Keuls post hoc test. (*D*) Western blot analysis of PTEN from HEK293 coexpressing *PTEN* coding sequences fused to 2-kb 3′-UTR containing either WT or mutated (Mut) *miR-23a* binding elements together with *miR-23a* as indicated. Quantitative expression levels of PTEN were obtained from three independent experiments and presented as ratio of means ± SEM, $n = 4$, and nromalized to control. $^{*}P < 0.05$, compared with vector control; $^{\dagger}P < 0.05$ compared with WT; one-way ANOVA with Newman–Keuls post hoc test.

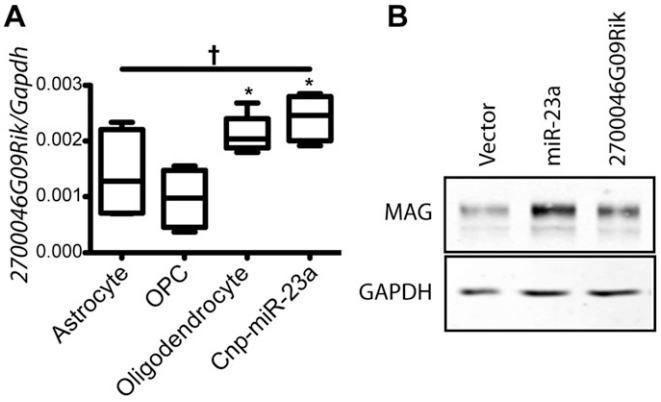

Fig. S6. (*A*) Relative RNA levels of *2700046G09Rik* in cultured astrocytes, OPC, or OL purified from either C57BL/6 or *Cnp–miR-23a* mice in differentiation conditions for 4 d. Data represent means ± SEM, $n = 4$. *$P < 0.05$ compared with OPC, $^{\dagger}P < 0.05$ compared with astrocytes; one-way ANOVA with Newman–Keuls post hoc test. (*B*) Representative Western blot analysis is shown of MAG from OPCs overexpressing *miR-23a* or *2700046G09Rik* as indicated.

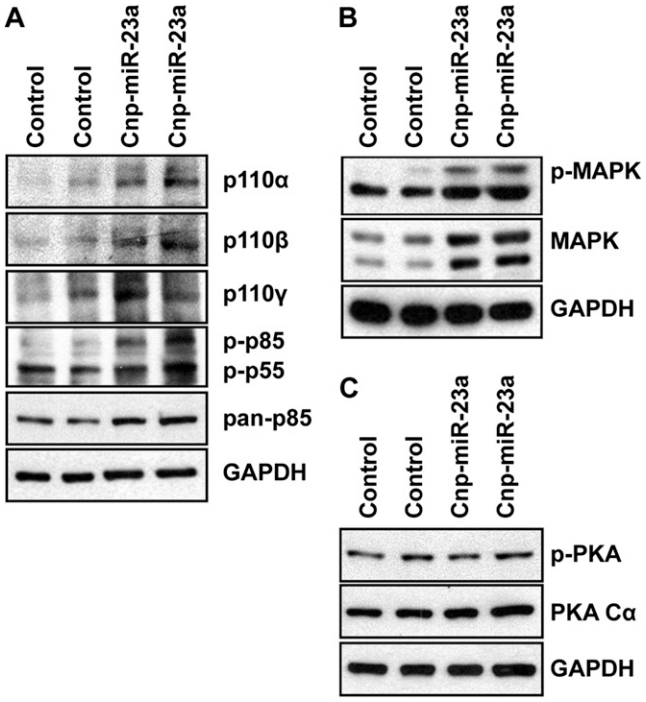

Fig. S7. *miR-23a* overexpression leads to activation of Akt/mTOR and MAPK pathways. (*A*) Western blot analysis of components in the PI3K pathway: p110α, p110β, p110γ, phosphorylated-p85 (p-p85), phosphorylated p55 (p-p55), and pan-p85 in OPCs purified from wild-type (control) and *Cnp–miR-23a* mice cultured for 4 DIV in differentiation medium. (*B* and *C*) Western blot analysis of p44/p42 MAPK (*B*) or PKA pathway (phosphorylated PKA and PKA Cα) (*C*) from OPCs purified from wild-type (control) or *Cnp–miR-23a* mice cultured for 4 DIV in differentiation medium.

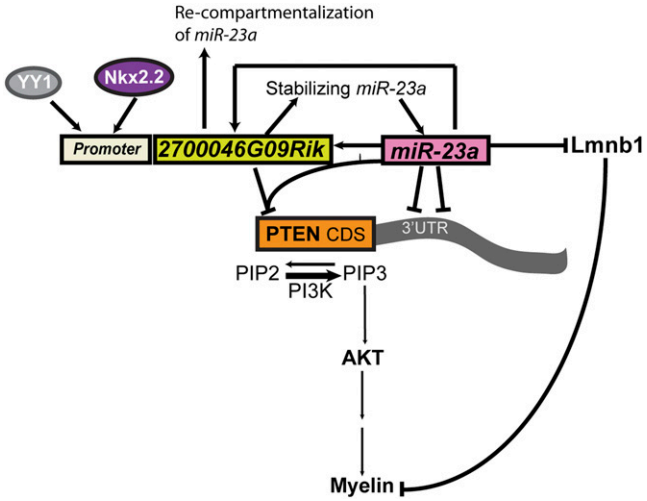

Fig. S8. Model for the mechanism of *miR-23a* in regulating myelination. *miR-23a* enhances *2700046G09Rik* and represses PTEN in oligodendroglia. *2700046G09Rik* interacts and stabilizes *miR-23a* as well as altering its cellular localization, which further enhances repressive effects of *miR-23a* on PTEN. Less PTEN in antagonizing PI3K activity leads to AKT activation, which results in myelination. *miR-23a* represses Lmnb1, leading to increased myelination.

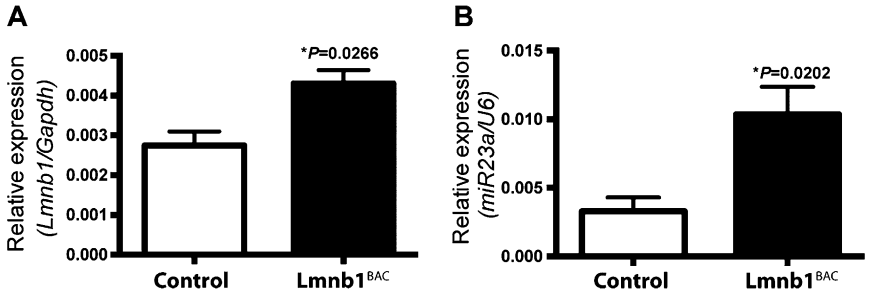

Fig. S9. Up-regulation of *miR-23a* in the murine model of autosomal dominant adult-onset leuokodystrophy (ADLD). Expression levels of *Lmnb1* (*A*) and *miR-23a* (*B*) in corpus callosum derived from the murine model of ADLD at P360, which is engineered to overexpress *Lmnb1*. Data represent means ± SEM, n = 4, 6 for control, or *Lmnb1*^{BAC} per genotype. *$P < 0.05$, unpaired Student t test.

Other Supporting Information Files

Dataset S1 (XLSX)
Dataset S2 (XLSX)